



Influences of downward transport and photochemistry on surface ozone over East Antarctica during austral summer: in situ observations and model simulations

Imran A. Girach^{1,2*}, Narendra Ojha³, Prabha R. Nair^{4,2}, Kandula V. Subrahmanyam^{5,2},
5 Neelakantan Koushik⁶, Mohammed M. Nazeer⁶, Nadimpally Kiran Kumar⁶, Surendran Nair
Suresh Babu⁶, Jos Lelieveld⁷, and Andrea Pozzer^{7,8*}

¹Space Applications Centre, Indian Space Research Organisation, Ahmedabad 380015, India

²Formerly at Space Physics Laboratory, Vikram Sarabhai Space Centre, Thiruvananthapuram 695022, India

³Space and Atmospheric Sciences Division, Physical Research Laboratory, Ahmedabad 380009, India

10 ⁴TC 95/1185, Aiswarya Gardens, Kumarapuram, Thiruvananthapuram - 695011, India

⁵National Remote Sensing Centre, Indian Space Research Organisation, Hyderabad 500015, India

⁶Space Physics Laboratory, Vikram Sarabhai Space Centre, Thiruvananthapuram 695022, India

⁷Department of Atmospheric Chemistry, Max Planck Institute for Chemistry, Mainz 55128, Germany

⁸Climate and Atmosphere Research Center, The Cyprus Institute, Nicosia, Cyprus

15

*Correspondence to: Imran A. Girach (imran.girach@gmail.com) and Andrea Pozzer (andrea.pozzer@mpic.de)

Abstract. Studies of atmospheric trace gases in remote, pristine environments are critical for
20 assessing the accuracy of climate models and advancing our understanding of natural processes
and global changes. We investigated the surface ozone (O₃) variability over East Antarctica during
the austral summer of 2015–2017 by combining surface and balloon-borne measurements at the
Indian station Bharati (69.4° S, 76.2° E, ~35 m above mean sea level) with EMAC atmospheric
chemistry-climate model simulations. The model reproduced the observed surface O₃ level (18.8
25 ± 2.3 nmol mol⁻¹) with negligible bias and captured much of the variability (R=0.5). Model
simulated tropospheric O₃ profiles were in reasonable agreement with balloon-borne
measurements (mean bias: 3–11 nmol mol⁻¹). Our analysis of a stratospheric tracer in the model
showed that about 40–50% of surface O₃ over the entire Antarctic region was of stratospheric
origin. Events of enhanced O₃ (~4–10 nmol mol⁻¹) were investigated by combining O₃ vertical
30 profiles and air mass back trajectories, which revealed the rapid descent of O₃-rich air towards the
surface. The photochemical loss of O₃ through its photolysis (followed by H₂O+O(¹D)) and
reaction with hydroperoxyl radicals (O₃+HO₂) dominated over production from precursor gases
(NO+HO₂ and NO+CH₃O₂) resulting in overall net O₃ loss during the austral summer.
Interestingly, the east coastal region, including the Bharati station, tends to act as a stronger
35 chemical sink of O₃ (~190 pmol mol⁻¹ d⁻¹) than adjacent land and ocean regions (by ~100 pmol



$\text{mol}^{-1} \text{d}^{-1}$). This is attributed to reverse latitudinal gradients between H_2O and $\text{O}(^1\text{D})$, whereby O_3 loss through photolysis ($\text{H}_2\text{O} + \text{O}(^1\text{D})$) reaches a maximum over the east coast. Further, the net photochemical loss at the surface is counterbalanced by downward O_3 fluxes, maintaining the observed O_3 levels. The O_3 diurnal variability of $\sim 1.5 \text{ nmol mol}^{-1}$ was a manifestation of combined
40 effects of mesoscale wind changes and up- and downdrafts, in addition to the net photochemical loss. The study provides valuable insights into the intertwined dynamical and chemical processes governing the O_3 levels and variability over East Antarctica.

1 Introduction

Tropospheric ozone (O_3) plays a pivotal role in governing the atmospheric oxidation
45 capacity, and influences air quality and climate warming (Seinfeld and Pandis, 1998). The major source of O_3 in the troposphere is its photochemical formation involving precursors such as nitrogen oxides (NO_x), carbon monoxide (CO) and non-methane hydrocarbons (NMHCs; Lelieveld and Dentener, 2000). The contribution of downward transport from the stratosphere is generally minor near the surface, although it can be significant at middle to high latitudes (Stohl
50 et al., 2003). Numerous studies have investigated the chemistry and dynamics of tropospheric O_3 and the roles of local to synoptic-scale processes (e.g., boundary layer height variation, horizontal and vertical transport, etc.; Nguyen et al., 2022; Young et al., 2018). Investigations of O_3 variations in remote pristine environments, isolated from major anthropogenic influences, are essential to understand the global changes in atmospheric composition, the role of natural processes including
55 downward transport from the stratosphere, and photo-denitrification of the snowpack (Jones et al., 2001). In this regard, the observations over environments such as Antarctica are extremely valuable and can provide insights into the global background atmosphere, besides providing data to test the results of chemistry-climate models. The mean surface O_3 over the Antarctic region was observed to be lower by nearly 5 nmol mol^{-1} than that over the Arctic polar region (Helmig et al.,
60 2007). Surface O_3 shows a pronounced seasonality ($\sim 15\text{--}20 \text{ nmol mol}^{-1}$ amplitude) with a summer minimum and a winter maximum over Antarctica, accompanied by periodic fluctuations associated with long-range transport (Kumar et al., 2021; Legrand et al., 2016; Oltmans and Komhyr, 1976; Winkler et al., 1992). In line with global increases in tropospheric O_3 due to the enhanced anthropogenic emissions since the pre-industrial era and impacts of climate warming



65 (Wang et al., 2022; Murazaki and Hess, 2006; Lelieveld et al., 2004), an increasing trend (<0.2
nmol mol⁻¹ y⁻¹) in surface O₃ has also been reported from Antarctica (Kumar et al., 2021).

Previous studies have investigated the long-term, inter-annual, seasonal and diurnal
variations in surface O₃ over Antarctica (Legrand et al., 2009, 2016), as well as the role of
horizontal transport (Tian et al., 2022) and chemistry including that of radicals (Preunkert et al.,
70 2012), halogen driven O₃ depletion (Tarasick and Bottenheim, 2002; Jones et al., 2013), and
stratospheric intrusions (Das et al., 2020). Antarctic observations have provided evidence of
widespread O₃ production during austral spring and summertime, affecting all stations through
horizontal mixing. This O₃ production contributes to a significant enhancement in annual mean O₃
over the Antarctic plateau (Helmig et al., 2007). While a weak coupling between stratospheric and
75 tropospheric O₃ was inferred earlier (Oltmans and Komhyr, 1976), frequent stratospheric
intrusions in this region were also reported (Cristofanelli et al., 2018; Das et al., 2020; Greenslade
et al., 2017). There have been extensive studies on a range of species utilizing datasets from
dedicated campaigns and projects over West Antarctica and South Pole (CHABLIS—Chemistry
of the Antarctic Boundary Layer and the Interface with Snow, Jones et al., 2008;
80 ISCAT—Investigation of Sulfur Chemistry in Antarctica, Davis et al., 2004; ANTCI—Antarctic
Tropospheric Chemistry Investigation (Eisele et al., 2008); WAIS—West Antarctic Ice Sheet, Frey
et al., 2005; Masclin et al., 2013). The variability of volatile organic compounds (VOCs), radicals,
O₃ and its precursors has been investigated over the East Antarctic plateau and eastern coastal
Antarctica (OPALE—Oxidant Production over Antarctic Land and its Export; Preunkert et al.,
85 2012 and references therein). But the east coast of Antarctica remains a relatively less explored
region as compared to west Antarctica and the South Pole.

The east coast of Antarctica is distinct from the west coast as well as the inland region of
Antarctica. Relatively high levels of hydroxyl and peroxy radicals over eastern Antarctica
(Dumont d'Urville; 66.67° S, 140.02° E, 40 m above mean sea level—amsl) during austral summer
90 (Kukui et al., 2012) indicate chemical differences from west Antarctica (Palmer; 64.77° S; 64.05°
W) where radical concentrations are lower. Short-term events of O₃ enhancements are observed
over the coastal as well as inland regions with higher frequency during the summer season and
they are associated with ultraviolet radiation reaching the surface, photochemical production and
transport (Crawford et al., 2001; Frey et al., 2015; Cristofanelli et al., 2018; Legrand et al., 2016).



95 Net summertime O₃ production (4–5 nmol mol⁻¹ d⁻¹) has been observed at the eastern coastal
Antarctica through NO_x emission from snow (Legrand et al., 2009, 2016). In contrast, surface or
boundary layer O₃ depletion are also observed mainly due to halogen chemistry involving iodine,
bromine and chlorine oxides, being more frequent in west Antarctica (Saiz-Lopez et al., 2007;
Simpson et al., 2007). Weaker or less frequent surface O₃ depletion is observed over the east coast
100 compared to the west coast of Antarctica (Jones et al., 2013; Legrand et al., 2016).

Most studies of East Antarctica have been based on in situ measurements of various trace
gases including radical species (O₃, NO, HONO, OH, DMS, BrO, etc.) at Dumont d'Urville,
Syowa (69.00° S; 39.58° E, ~29 m amsl) and Zhongshan (69.37° S, 76.36° E, 18.5 m amsl; Kukui
et al., 2012; Legrand et al., 2016, 2009; Murayama et al., 1992; Tian et al., 2022) stations. These
105 studies have shown the surface O₃ variability on different scales (i.e., diurnal: ~2 nmol mol⁻¹,
seasonal: ~18 nmol mol⁻¹, and long-term trend: 0.07±0.07 nmol mol⁻¹ y⁻¹). Only few studies have
analyzed the relevant larger-scale trace gas distributions and discussed the model performance of
seasonal changes in surface O₃ or tropospheric O₃ (Wang et al., 2022; Griffiths et al., 2021),
including halogen chemistry (Yang et al., 2005; Fernandez et al., 2019). Studies investigating the
110 chemistry and dynamics of surface O₃ are scarce for Antarctica (Morgenstern et al., 2013). To the
best of our knowledge, there are no comprehensive studies discussing the surface O₃ variability
and associated processes based on the synergy of in situ measurements and chemistry-climate
modeling over East Antarctica. It is timely to investigate the underlying processes since an
increasing O₃ trend has been reported over this part of the world recently (Kumar et al., 2021).

115 Our study aims to contribute to the understanding of chemical and dynamical processes
governing the surface O₃ variability over the east coast of Antarctica. We have conducted in-situ
measurements during three different years and performed simulations using a global chemistry-
climate model to unravel the atmospheric processes that control the summertime O₃ levels and
variability. Details of the measurements and model simulations are given in the next section.
120 Results of the O₃ variability and a comparison of model results with measurements, and an analysis
of photochemical and dynamical contributions are presented in section 3. A summary, the main
conclusions, and a future outlook are presented in section 4.



2 Measurements and model simulations

125 2.1 In situ measurements

Surface O₃ was measured at the Indian station Bharati (69.4° S, 76.2° E, ~35 m above mean sea level) at the Larsemann Hills in the east coast of Antarctica during the summer seasons of three years 2015–2017: 29 January–13 February 2015, 17 January–24 February 2016, and 11 December 2016–16 February 2017. The Bharati site experiences a surface pressure of ~980±10 hPa, cold
130 temperatures (-0.1±3 °C; -11–8 °C), moderate humidity (60±13.5%; 34–98%) and mainly easterly winds with a number of blizzards during the summer season. A detailed overview of the meteorological conditions at Bharati station can be found in Soni et al., 2017.

Surface O₃ mixing ratios were measured using an online ultraviolet photometric ozone analyzer manufactured by the Environnement S.A, France (model O342). The instrument derives
135 O₃ mixing ratios using the Beer–Lambert law considering the absorption of ultraviolet radiation around 253.7 nm by O₃ molecules. The measurement noise, lower detection limits, linearity and minimum response time are 0.5 nmol mol⁻¹, 1 nmol mol⁻¹, ±1 % and 10 s, respectively. The instrument was operated on the auto-response mode (response time of 10–90 s) under permissible range of temperature. O₃ mixing ratios were recorded continuously at 5 min averaging intervals.
140 Air samples were drawn from a height of approximately 2 m above the ground level through a Teflon tube and filtered through 5 μm non-reactive polytetrafluoroethylene dust filter prior to injection into the analyzer. Prior to each expedition, the analyzer was calibrated for mixing ratios of 20 and 30 nmol mol⁻¹ using a multichannel calibrator. The measurement uncertainty is estimated to be ~5 % (Tanimoto et al., 2007). In addition to measurements at Bharati, surface O₃ at Syowa
145 and Arrival Heights (77.80° S; 166.67° E) available from <https://ebas-data.nilu.no/Default.aspx> for the study period are also used for the comparison of model results.

The vertical profiles of O₃ partial pressure were measured using balloon-borne electrochemical ozonesondes manufactured by the En-Sci Corporation, USA (Model: 2Z-V7). A total of 12 profiles were measured during the study period. The O₃ partial pressure was converted
150 to O₃ mixing ratios using the simultaneously measured atmospheric pressure by radiosonde (model: iMet-1-RSB). Air is passed through an electrochemical concentration cell (ECC) using a built-in non-reactive pump, and the current generated by the electrochemical reaction of O₃ (with



potassium iodide) is measured by an electronic interface board and converted into an O₃ partial pressure. The detailed operation principle and performance evaluation of ozonesonde instrument
155 are described in Komhyr et al., 1995 and references therein. The accuracy of O₃ measurements is reported to be 5–10% up to an altitude of 30 km (Smit et al., 2007). Additional details of the O₃ measurements and meteorological parameters using this technique can be found elsewhere (Ajayakumar et al., 2019; Ojha et al., 2014). Besides our measurements at Bharati, we utilized available O₃ vertical profiles measured using ECC ozonesondes at Davis station (68.58° S 77.97°
160 E; https://data.aad.gov.au/metadata/records/AAS_4293_Ozonesonde) in this study.

The surface level wind speed and direction were measured using an automatic weather station, which meets the standards of the World Meteorological Organization and was operated by the India Meteorological Department. Wind direction measurements are used here to analyze the changes in surface O₃ on a diurnal time scale. To understand the impacts of updraft and downdrafts,
165 the vertical wind at the surface was measured using a fast response ultrasonic anemometer (make: METEK, GmbH, Germany; model: USA-1 Scientific). The factory calibrated sensor was mounted at 3 m level above the ground and was operated at 25 Hz during January 2016. The measuring resolution and accuracy of the vertical velocity are $\pm 0.01 \text{ m s}^{-1}$ and 0.2 m s^{-1} , respectively. Further details on the instrument can be found in (Reddy et al., 2021)

170 2.2 Model simulations

In this work the EMAC (ECHAM5/MESSy Atmospheric Chemistry) model (Jöckel et al., 2010, 2006) has been used. This model is a numerical chemistry and climate simulation system that includes sub-models describing tropospheric and middle atmospheric processes and their interaction with oceans, land and human influences. It uses the second version of the Modular
175 Earth Submodel System (MESSy2) to link multi-institutional computer codes. The core atmospheric model is the 5th generation European Centre Hamburg general circulation model (ECHAM5, Roeckner et al., 2006). The physics subroutines of the original ECHAM code have been modularized and reimplemented as MESSy submodels and have continuously been further developed. Only the spectral transform core, the flux-form semi-Lagrangian large scale advection
180 scheme, and the nudging routines for Newtonian relaxation are remaining from ECHAM5. For the present study we applied EMAC (MESSy version 2.55.0) in the T106L47MA-resolution, i.e. with



a spherical truncation of T106 (corresponding to a quadratic Gaussian grid of approximately $1.1^\circ \times 1.1^\circ$ in latitude and longitude) with 47 vertical hybrid pressure levels up to 0.01 hPa. In this work we used the same set up as in Reifenberg et al. (2022), and the model results encompass the
185 years 2014–2018 with a 3-hours output frequency. Global atmospheric chemistry models are known to overestimate tropospheric ozone (Young et al., 2018), and EMAC is no exception to this. Nevertheless, extensive ozone evaluation (Jöckel et al., 2016) shows that the EMAC model has a very low (less than 10%) or no bias in the troposphere against observations for latitudes below 60° S. Furthermore, the EMAC model has been extensively evaluated in the last years both
190 for the gas phase (Jöckel et al., 2016; Taraborrelli et al., 2021) and for the aerosol phase (Pozzer et al., 2012; Brühl et al., 2018; Pozzer et al., 2022).

To investigate the effects of transport, air mass back trajectories have been computed using the HYSPLIT (HYbrid Single Particle Lagrangian Integrated Trajectory) model version-4 (Rolph et al., 2017; Stein et al., 2015) with the input of $1^\circ \times 1^\circ$ gridded GDAS (Global Data Assimilation
195 System) meteorological data.

3 Results and Discussions

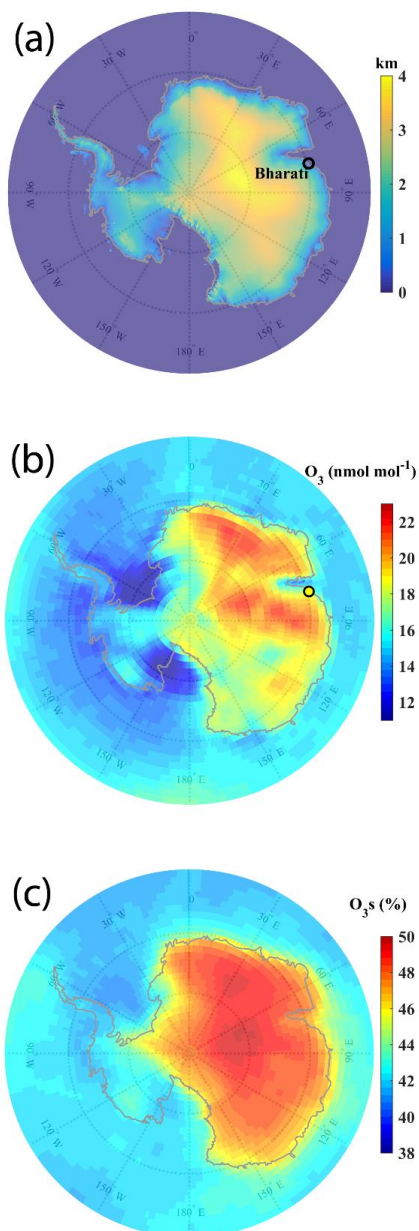
3.1 O₃ variability: comparison of observations with model simulations

Figure 1a shows the elevation map of Antarctica marked with the location of the Indian station Bharati (69.4° S, 76.2° E, ~ 35 m amsl), where surface-based and balloon-borne
200 measurements of O₃ have been conducted during this study. The surface elevation is higher (up to 4 km) over the eastern part of Antarctica. Figure 1b shows the spatial distribution of surface O₃ during summer of 2015–2017 (29 January–13 February 2015, 17 January–24 February 2016, and 11 December 2016–16 February 2017) as simulated by the EMAC model, along with the mean observed value at Bharati station (18.8 ± 2.3 nmol mol⁻¹). The mean O₃ distribution shows increase
205 from the oceanic region (10 – 16 nmol mol⁻¹) to the landmass (15 – 23 nmol mol⁻¹), nearly following the topographical features of Antarctica. Overall, the model simulated spatial distribution of O₃ (Fig. 1b) is seen to be in agreement with the distribution based on measurements from different stations (Fig. S1). This is further consistent with previous studies showing higher O₃ mixing ratios over elevated sites (Summit; 3212 m amsl and South Pole; 2830 m amsl) as compared to the



210 coastal/oceanic region (Helmig et al., 2007). The balloon-borne observations (Fig. 3) also show
increase in mean O₃ mixing ratios with altitude.

Figure 1c shows the stratospheric contribution (in percent) to the surface O₃ based on the
stratospheric O₃ tracer in the model (O_{3s}). O_{3s} is seen to contribute by 40–50% over the Antarctic
region with greater contribution (45–50%) over the continent with higher elevation than that over
215 the surrounding ocean (40–45%). The mean stratospheric contribution at the observation site
Bharati is estimated to be ~47% (~9 nmol mol⁻¹), showing that nearly half of O₃ at the surface is
of the stratospheric origin. Mihalikova and Kirkwood, 2013 have estimated a 6–7% occurrence
rate of tropospheric folds (1–2 folds month⁻¹) during summer using radar observations at Troll
station (72.0° S, 2.5° E, 1275 m amsl). In another recent study also, the enhancement by 20–30
220 nmol mol⁻¹ (67–100% as compared to the climatological mean) is seen in upper tropospheric O₃
above Bharati station due to stratospheric intrusions (Das et al., 2020). Therefore, stratospheric
intrusions are suggested to transport the O₃-rich airmasses to the troposphere, which subsequently
descend to the surface and get redistributed across the region through horizontal transport. Descent
of O₃-rich airmasses is further discussed in section 3.2.



225

Figure 1. (a) Elevation map of Antarctica along with the location of the Indian station Bharati marked by a black circle. (b) Spatial distribution of surface O_3 simulated by the EMAC model, averaged over the study period. Colour in the black circle in (b) represents the mean value from



the in situ measurements at Bharati. (c) Percent contribution of stratospheric O₃ to the surface O₃ derived from the EMAC model during the study period.

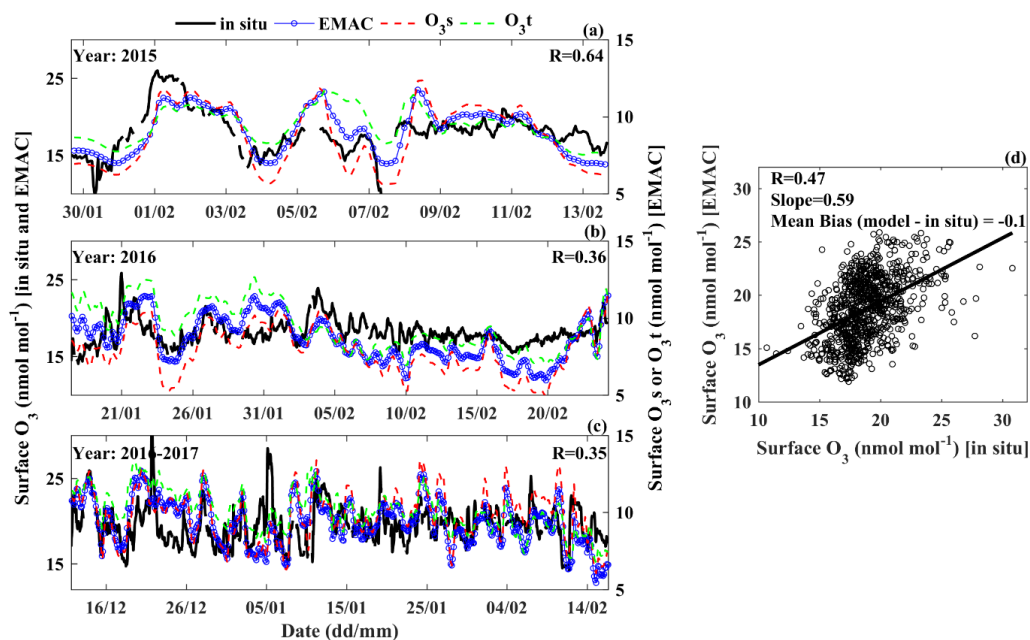


Figure 2. Variability in surface O₃ (a-c) at Bharati during austral summer of 2015–2017 based on in situ measurements (black) and EMAC simulations (blue). Green and red curves show the absolute stratospheric (O_{3s}) and tropospheric (O_{3t}) contributions to the surface O₃. A scatter plot between in situ measurements and model simulated O₃ is shown in (d).

Figure 2a–c shows the variations in surface O₃ at Bharati station from in situ measurements and model simulations during the summer seasons of 2015–2017. The mean O₃ levels estimated from the model simulations (18.7 ± 3.0 nmol mol⁻¹) are in very good agreement with the measurements (18.8 ± 2.3) with negligible bias at this station. Further, the surface O₃ level at Bharati is observed to be similar to an earlier observation (~ 13 – 20 nmol mol⁻¹) at this station (Ali et al., 2017) and also to other stations in the coastal region of East Antarctica (Fig. S1). The model tends to successfully capture several features of the observed variability (Fig. 2a–c), nevertheless the overall correlation coefficient is 0.47 (Fig. 2d). The comparison for two other coastal stations, Syowa and Arrival Heights during the same study period also shows that the model can reproduce the summertime O₃ levels with small bias and the temporal variability moderately well (Fig. S2–3). The blue and green curves in Fig. 2 show the individual contributions from stratospheric (O_{3s})



and tropospheric sources ($O_{3t}=O_3$ minus O_{3s}), respectively. Both stratospheric and tropospheric sources are estimated to be contributing nearly equally, 47% and 53%, respectively. Further, the stratospheric and tropospheric O_3 at the surface are seen to be strongly correlated ($R=0.9$; figure not shown) over most of the region mainly due to the mixing of stratospheric and tropospheric airmasses during the transport from the tropopause to the surface. Strong local O_3 production (e.g., through NO_x from snow) or direct transport of stratospheric air would decrease the correlation or perturb the variations in O_{3s} and O_{3t} . Overall, similar variability of comparable magnitude in O_{3s} and O_{3t} indicate the absence of strong “local” production or “direct” stratospheric transport to the surface. However, about 50% stratospheric contribution to surface O_3 points to significant stratospheric intrusions over the Antarctic region.

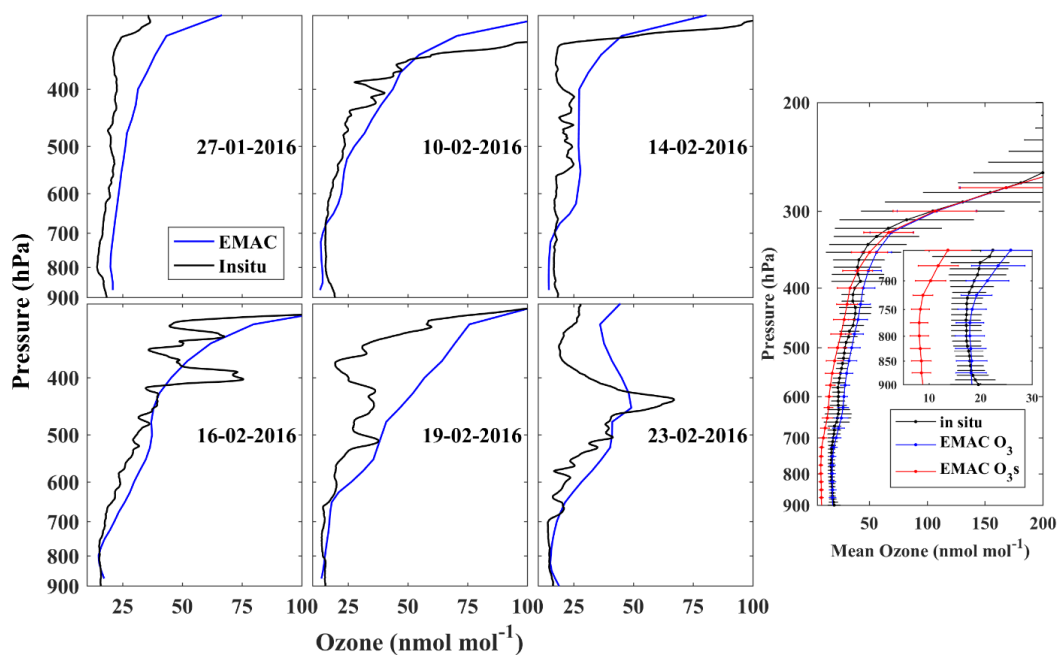


Figure 3. Vertical profiles of O_3 over Bharati station during a few representative days, based on the in situ measurements (black) and EMAC simulation (blue). The insert on the right shows the mean vertical distribution of O_3 and O_{3s} (red) corresponding to 12 profiles during the study period.

Figure 3 shows the comparison of balloon-borne observations of O_3 vertical profiles with model simulation over Bharati station in 2016. Out of twelve, six individual representative profiles are shown in the figure. O_3 mixing ratios gradually increase with altitude up to the tropopause



(~8.5 km; ~300 hPa), showing also O₃ peaks in the middle/upper troposphere during some days.

265 The model successfully captures the mean vertical distribution especially in the lower troposphere (pressure > ~700 hPa) with a mean bias of less than 3 nmol mol⁻¹. There is an agreement between the model and observations in the upper troposphere, however, the model overestimates O₃ levels (by ~11 nmol mol⁻¹) at the tropopause. Ozone-sonde measurements from another station in the region, Davis (68.6° S, 78.0° E), were also compared with the model results for the study period

270 (Fig. S4 and S5). The O₃ variability from model results (standard deviation: 3–13 nmol mol⁻¹) is comparable or slightly lower than the observed variability in the vertical distribution (950–350 hPa). The O₃s contribution is ~45–50% in the lower troposphere (pressure > ~700 hPa) but increases with altitude to 65% at 500 hPa up to 100% at and above the tropopause (~300 hPa). The EMAC model captures both the mean vertical structure as well as some secondary O₃ peaks (e.g.,

275 23 February 2016; Fig. 3) in the upper troposphere (~6 km; 450 hPa). However, there are some noticeable differences between model and observations on individual days (e.g., 19 February 2016; Fig. 3). The model limitation in reproducing some features of secondary peaks have been suggested to be due to coarser vertical resolution and the temporal differences (Ojha et al., 2017), and confirmed recently in a study focusing on tropopause folding frequency (Bartusek et al., 2023).

280 Overall, the model reproduces the observed tropospheric O₃ distribution and most of the day-to-day variability in the surface and tropospheric O₃. It is to be noted that the performance of global chemistry-climate models is also limited by the parameterization schemes developed for such pristine environments with extreme climatic conditions (e.g., frequent blizzards). Nevertheless, our study fills a gap with respect to the evaluation of the widely applied EMAC model for the

285 Antarctic region and the results may have implications to further improve the model in future studies.

3.2 Influences of downward transport on surface O₃

Several events of surface O₃ enhancements were observed during the study period, as illustrated in Fig. 2. Two such events on 23 February 2016 and 01 February 2015 are investigated

290 in detail to understand the mechanism driving such variability.

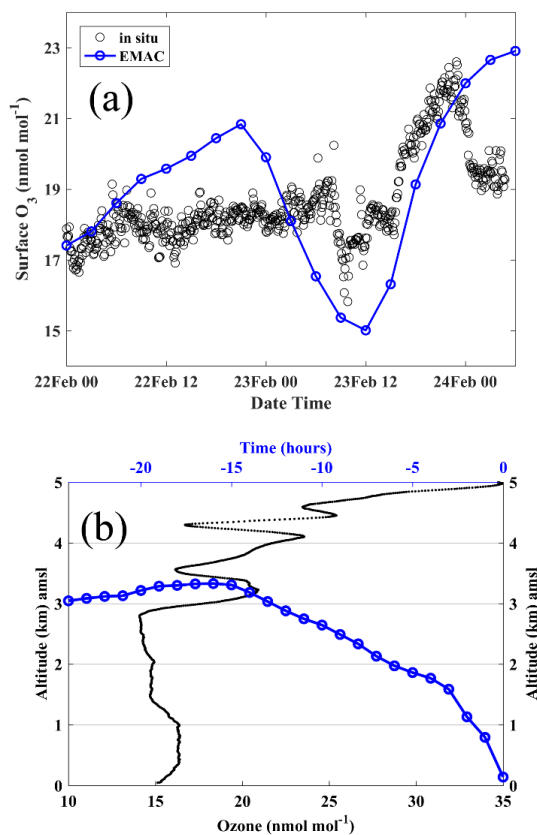


Figure 4. (a) surface O_3 variations at Bharati station depicting an event of significant O_3 enhancement around 23:00 local time on 23 February 2016. (b) Variations in the altitude of air mass (blue) along the backward trajectory with respect to time from the O_3 enhancement event. Vertical profile of O_3 measured around 11:00 on 23 February 2016 (black).

Figure 4a shows that surface O_3 over Bharati was enhanced sharply by $\sim 4 \text{ nmol mol}^{-1}$ around 23:00 on 23 February 2016. Backward air mass trajectories show that this air mass originated from $\sim 3 \text{ km}$ altitude about 12 hours before the event. The balloon-borne O_3 vertical profile obtained at that time (11:00 on 23 February 2016; Fig. 4b) shows the presence of a layer with enhanced O_3 ($\sim 22 \text{ nmol mol}^{-1}$) relative to lower altitudes ($\sim 15 \text{ nmol mol}^{-1}$). Based on these collocated observations and trajectory simulations, it is suggested that the O_3 rich air from this layer descended to the surface over Bharati in ~ 12 hours with a descent rate of $>250 \text{ m h}^{-1}$ (0.07 m s^{-1}). The estimated descent velocity seems to be consistent with the in situ measured mean vertical wind



speed ($0.09 \pm 0.29 \text{ m s}^{-1}$) measured at this station during 18–29 January 2016. The O_3 enhancement
305 observed in the upper troposphere ($\sim 6 \text{ km}$; see Fig. 3) on 23 February 2016 is associated with a
stratospheric intrusion (Das et al., 2020). The presence of the jet-stream in the vicinity of the
tropopause ($\sim 9 \text{ km}$ altitude; $\sim 300 \text{ hPa}$) can enhance the turbulence due to strong wind shear
(squared wind shear = $5 \times 10^{-4} \text{ s}^{-2}$). Along with this turbulence, tropopause oscillations led to the
stratospheric intrusion during 22–23 February 2016 (Das et al., 2020). The presence of similar
310 surface O_3 enhancement events on several other days also (Fig. 2) suggests that this is a periodic
phenomenon that significantly contributes to tropospheric O_3 in the region.

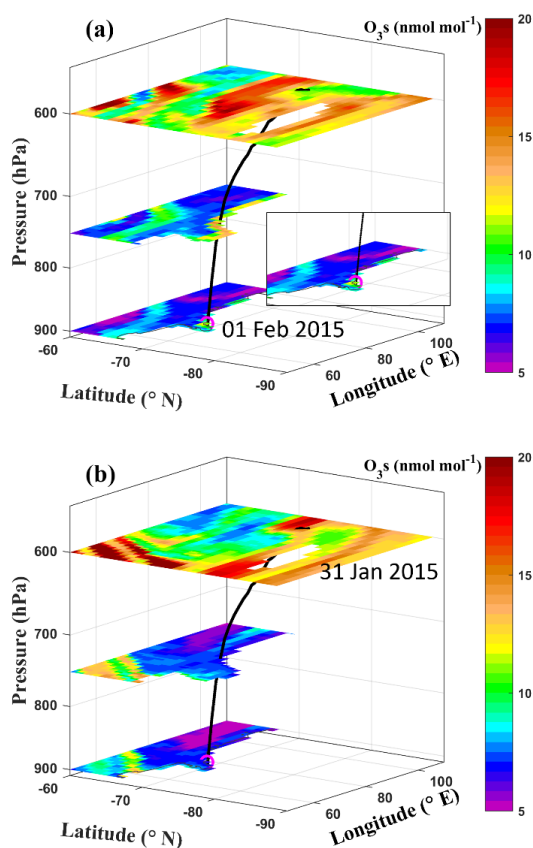


Figure 5. Spatial distribution of the stratospheric O_3 tracer in the model at different pressure levels
for (a) 01 February 2015 depicting an enhancement at surface, and (b) 31 January 2015 depicting
315 an enhancement in the upper troposphere. The black curve represents a 24-hour backward air mass



trajectory ending at Bharati station (magenta circle) on 01 February 2015 and originating around 600 hPa on 31 January 2015.

Surface O_3 shows a continuous enhancement from about 12–14 nmol mol^{-1} on 31 January 2015 to about 25 nmol mol^{-1} on 01 February 2015 (Fig. 2a). To analyze the influence of transport from the stratosphere, the spatial distribution of the stratospheric O_3 tracer at different pressure levels is combined with air mass trajectories (Fig. 5). The insert in Fig. 5a shows a zoomed view of O_{3s} around Bharati station on 01 February 2015. The air mass backward trajectory ending at Bharati station at the time of the observed enhancement is shown by the black curve. The air mass is traced back to ~600 hPa (~4 km) one day prior to the observed enhancement (i.e., 31 January 2015) at a lower latitude, where a patch of stratospheric O_3 (20 nmol mol^{-1}) is simulated by the model. A clear descent of air mass with a descent rate of ~0.05 m s^{-1} is seen, leading to the enhancement in surface O_3 on 01 February 2015.

The above analysis of two representative events shows that the intrusion of stratospheric O_3 followed by descent of O_3 -rich air can cause a 4–10 nmol mol^{-1} enhancement in surface O_3 during the study period. The result is in line with a continuous increase in O_3 and O_{3s} with altitude, as shown in Fig. 1c and 3. Similar variations of O_{3t} compared to O_{3s} (Fig. 2) indicate significant air mass mixing during the transport process. O_3 enhancement events with similar magnitude were also observed at the nearby station Zhongshan (69.37° S 76.36° E; Ding et al., 2020; Tian et al., 2022) and with larger magnitude at South Pole (8–20 nmol mol^{-1} ; Oltmans et al., 2008) attributed to transport or NO_x driven cumulative photochemical production, assuming a marginal role of transport from the stratosphere or free-troposphere (Cristofanelli et al., 2018; Ding et al., 2020). The occurrence of such O_3 enhancement is less evident over the coastal regions compared to the Antarctic plateau (Jones, 2003). However, substantial contributions of stratosphere-troposphere exchange were associated with air mass fluxes up to 60 $\text{kg m}^{-2} \text{d}^{-1}$ (Sanak et al., 1985) using in situ measurement of Beryllium isotope at Dumont d'Urville station. Based on long-term balloon-borne measurements and GOES-Chem (Goddard Earth Observing System coupled with Chemistry) model simulations, Greenslade et al. (2017) also reported large stratosphere to troposphere O_3 fluxes ($0.50\text{--}0.75 \times 10^{17}$ molecules $\text{cm}^{-2} \text{month}^{-1}$) during summer, which exceed those during winter ($0.25\text{--}0.50 \times 10^{17}$ molecules $\text{cm}^{-2} \text{month}^{-1}$).



345 3.3 Influences of photochemistry on surface O₃

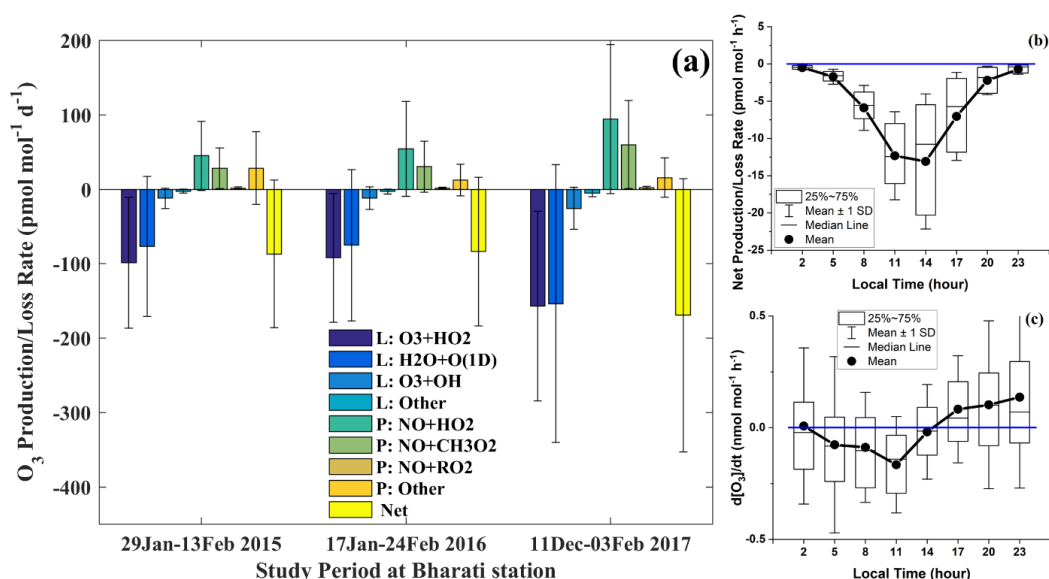


Figure 6. (a) Mean production and loss rates of surface O₃ through different chemical pathways at Bharati during the study period, (b) diurnal variation of net O₃ change due to photochemistry, derived from the EMAC model simulations, and (c) rate of change of surface O₃ (dO₃/dt) based on the in situ measurements at Bharati station.

The production and loss rates of O₃ through different chemical pathways have been estimated from the EMAC model simulation, and the mean values during the study period are shown in Fig. 6a. Among various production and loss reactions, O₃+HO₂ and H₂O+O(¹D) are found to be the dominant O₃ loss pathways, whereas NO+HO₂ and NO+CH₃O₂ are the major O₃ production reactions. Overall, the aforementioned chemical losses tend to dominate the production leading to a net photochemical loss in surface O₃ at Bharati. Effectively the study region acts as a net chemical sink of O₃. Note that loss through O₃+OH and other reactions, and production through NO+RO₂ and other reactions are relatively small in magnitude (Fig. 6). Dry deposition over ice and the surrounding ocean is a minor O₃ removal mechanism as well. The substantial variability (large error bars in Fig. 6a) in production and loss terms arises from the diurnal and day-to-day variations. Figure 6b-c shows the mean diurnal variation of net photochemical production or loss rates from the EMAC model and the rate of change of O₃ (i.e., dO₃/dt) from in situ measurements.



The net loss is relatively high during noontime (11–14 h) and negligibly small after 23:00 and prior to 5:00. In situ measured rate of change, dO_3/dt , is negative around 11:00 indicating overall
365 loss which includes the influences of both photochemistry as well as dynamics. The positive rate of change after 17:00 and prior to 5:00 represents an increase in O_3 mainly through horizontal or vertical transport as photochemistry is weak under conditions of low solar irradiance.

Despite of being a net photochemical sink of surface O_3 , it is observed that the levels of O_3 are relatively steady or continuous over time (Fig. 2c). We estimated surface O_3 fluxes by
370 multiplying the model simulated vertical wind with the O_3 concentration at the model level just above the surface. Figure 7b shows the mean O_3 flux averaged over the study period. The negative flux represents the number of O_3 molecules moving downward (contributing to surface O_3) per unit area and per unit of time. A stronger downward flux along the east coast (Fig. 7b) counterbalances the net photochemical O_3 loss (Fig. 7a). Assuming a boundary layer height of 500
375 m, the loss rates integrated over boundary layer are estimated at 2.7×10^{13} molecules $m^{-2} s^{-1}$, which is of comparable magnitude to the modelled downward flux (Fig. 7b). O_3 and O_3 fluxes (mean of fluxes at surface and a level above) correlate negatively ($R=-0.3$) at Bharati in the EMAC simulation, as shown in Fig. S6a. This is substantiated with a negative correlation of surface O_3 with the vertical wind (Fig. S6b), suggesting enhanced O_3 during conditions of descent. The results
380 suggest that despite the net chemical sink of O_3 , the surface O_3 is maintained by a flux from above during the summer over the coastal region. The O_3 loss through chemistry is counterbalanced by the contribution from dynamics (or vice versa) over East Antarctica during austral summer.

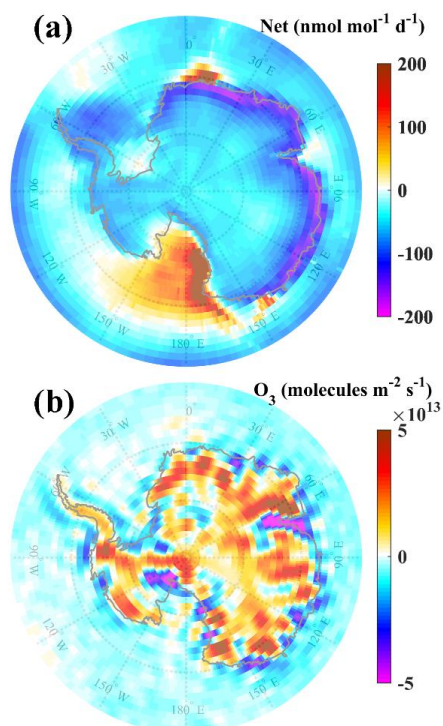
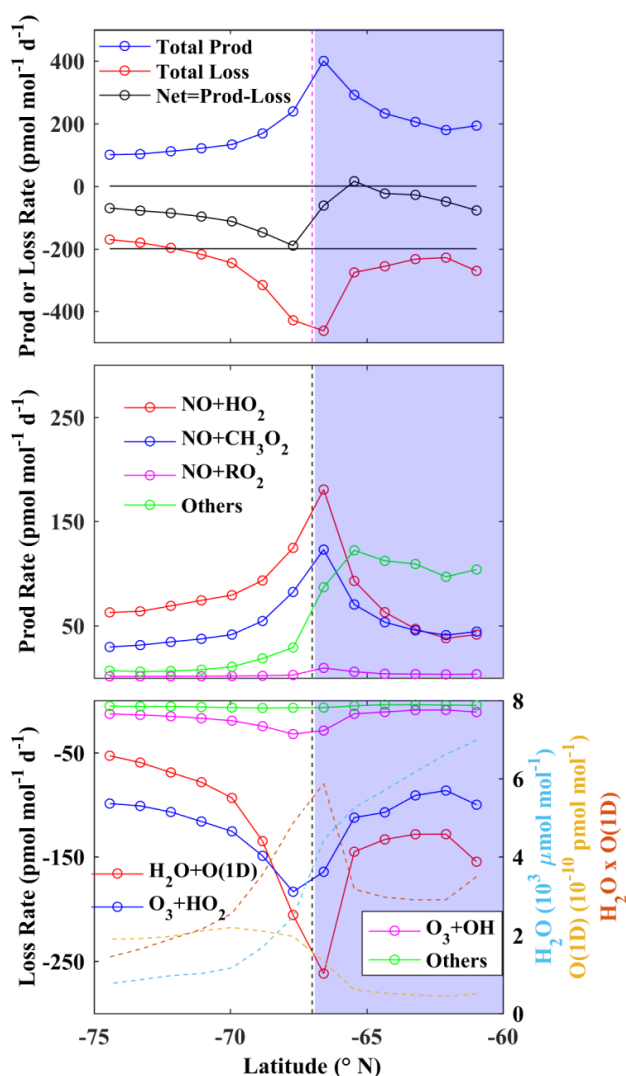


Figure 7. Spatial distribution of (a) net rate of change (production minus loss) of surface O₃ due
385 to photochemistry and (b) O₃ flux at surface averaged over the study period.

In order to understand whether the O₃ photochemical loss over the Bharati station also prevails over larger regions in Antarctica, we analyze the spatial distribution of net production or loss rates averaged during the austral summer (Fig. 7a). It is important to note that our simulations show that the entire Antarctic continent act as sink of O₃, in contrast to the previously reported net
390 O₃ production through NO emission from snow (Legrand et al., 2016 and references therein). In the east coastal Antarctic region O₃ loss rates are significantly higher (~190 pmol mol⁻¹ d⁻¹) suggesting that it acts as a relatively strong chemical sink of surface O₃. The loss rate is at peak (~190 pmol mol⁻¹ d⁻¹) over the east coast, higher by ~100 pmol mol⁻¹ d⁻¹ compared to adjacent land and ocean, and it gets further lower (~50 pmol mol⁻¹ d⁻¹) much away from the coast. Note that
395 model simulated mean OH and NO are in the range of 0.05–0.5 × 10⁶ molecules cm⁻³ and 0.5–10 pmol mol⁻¹, respectively, over entire the Antarctic region which is in line with earlier measurements at the west coast (OH mean: 0.11 × 10⁶ molecules cm⁻³, ranging <0.1–0.9 × 10⁶



400 molecules cm^{-3} ; NO: estimated value of 5 pmol mol^{-1}) by Jefferson et al., 1998 and Bloss et al., 2010, but lower (almost 5 times) than those measured during OPALE campaign (OH mean: 2.1×10^6 molecules cm^{-3} , ranging $<0.8\text{--}6.2 \times 10^6$ molecules cm^{-3} ; NO: $5\text{--}70 \text{ pmol mol}^{-1}$; Kukui et al., 2012).



405 **Figure 8.** Latitudinal variation of production, loss and net rates of changes of surface O_3 averaged along the east coastal longitudinal band of $15\text{--}130^\circ \text{ E}$ during January 2017. The blue areas represent the ocean environment and vertical dashed line shows the approximate coast line.



The net O₃ loss rate (Fig. 7a) is found to be lower over land than over ocean and is highest along the east coast. We further considered 6 grids at both sides of the coast line and averaged over the longitude range 15–130° E (i.e., East Antarctica). The variations in average production, loss and net rates with latitude are shown in Fig. 8. Since the latitude corresponding to different grids at 15–130° E are different, latitudes shown on the x-axis represent average latitudes. Thus, as we proceed from left to right (lower latitude to higher latitude) in Fig. 8, we move from land to ocean.

From Fig. 8a, it is clearly seen that the O₃ production as well as loss are maximum near the coast. Since loss dominates over the production, the net rate is negative with ~190 pmol mol⁻¹ d⁻¹. Figure 8b and c represent changes in different production and loss pathways across the coast. The photolytic O₃ loss, followed by H₂O+O(¹D), is found to be the dominating loss process peaking at ~300 pmol mol⁻¹ d⁻¹ along the coast. The reason for the peak loss rate at coast is related to the opposite latitudinal gradients in H₂O and O(¹D) (see Fig. 8c; right axis). H₂O is substantially higher (~6000 μmol mol⁻¹) over ocean but much lower (1000 μmol mol⁻¹) in the drier atmosphere above continent. In contrast, O(¹D) is higher (2 × 10⁻¹⁰ pmol mol⁻¹) over the continent primarily due to intense solar insolation at higher elevation and over the bright ice surface. Therefore, latitudinally opposite variations of H₂O and O(¹D) lead to a relative maximum in H₂O+O(¹D) near the coast. We also note that there is significant O₃ production over the ocean due to reactions other than the three primary reactions of peroxy radicals (HO₂, RO₂, CH₃O₂) with NO.

Under the prevailing relatively strong O₃ sink along the east coast, the mean O₃ level during summer is maintained by the downward flux of O₃ from the stratosphere.

3.4 Diurnal variation of surface O₃ at Bharati

Considering day-to-day variability, including enhancement events governed by stratospheric influence, ΔO₃ is computed by subtracting the running mean O₃ (288 points; 5 min interval—daily running mean) from the observed O₃. Figure 9a shows the mean diurnal variation of ΔO₃ during the 18 January–23 February 2016 period for which measurements of horizontal wind at surface were also available. Surface O₃ exhibits a diurnal variation, being relatively low during the afternoon (15:00 local time) and relatively high during nighttime (Fig. 9) with a diurnal amplitude of ~1.2 nmol mol⁻¹. Figure 9b shows the wind rose color coded with ΔO₃ mixing ratios. Sunlight at Bharati is abundant during summer and the land-sea thermal contrast explains the typical diurnal



435 change in the wind direction under normal meteorological conditions, i.e., excluding blizzards and
snow storms. Figure S7 shows time series of the wind direction and surface ΔO_3 , depicting the
link between O_3 and the wind direction. Due to higher O_3 over the eastern Antarctic land regions,
winds from that sector transport the O_3 -rich air to the Bharati station causing enhanced O_3 mixing
ratios. O_3 is higher when wind is parallel to the coast (easterly; wind direction $\sim 90^\circ$) or from the
440 land (wind direction: $90\text{--}240^\circ$). Under calm wind condition, the influence of transport is minimal
and photochemical loss is more pronounced. When the wind is weak and from the ocean (wind
direction: $30\text{--}90^\circ$ N), O_3 levels are lower due to dilution by mixing with air from the oceanic
sector. The O_3 diurnal variation is also closely linked with the vertical wind. Based on limited in
situ measurements of the vertical wind at the surface during 18–29 January 2016, the mean diurnal
445 variation of vertical wind (w) along with ΔO_3 is shown in Fig. 9c. Downdrafts and stronger
updrafts (up to $\sim 0.4\text{ ms}^{-1}$) are seen during nighttime (or lower solar zenith angle; 20:00–07:00) and
daytime (08:00–19:00), respectively. Higher O_3 during nighttime is associated with downdrafts
and O_3 mixing ratios are reduced with increasing updraft intensity. The EMAC model shows
limitations in reproducing the observed diurnal variation likely because of coarse resolution
450 averaging out the topography and mesoscale dynamics.

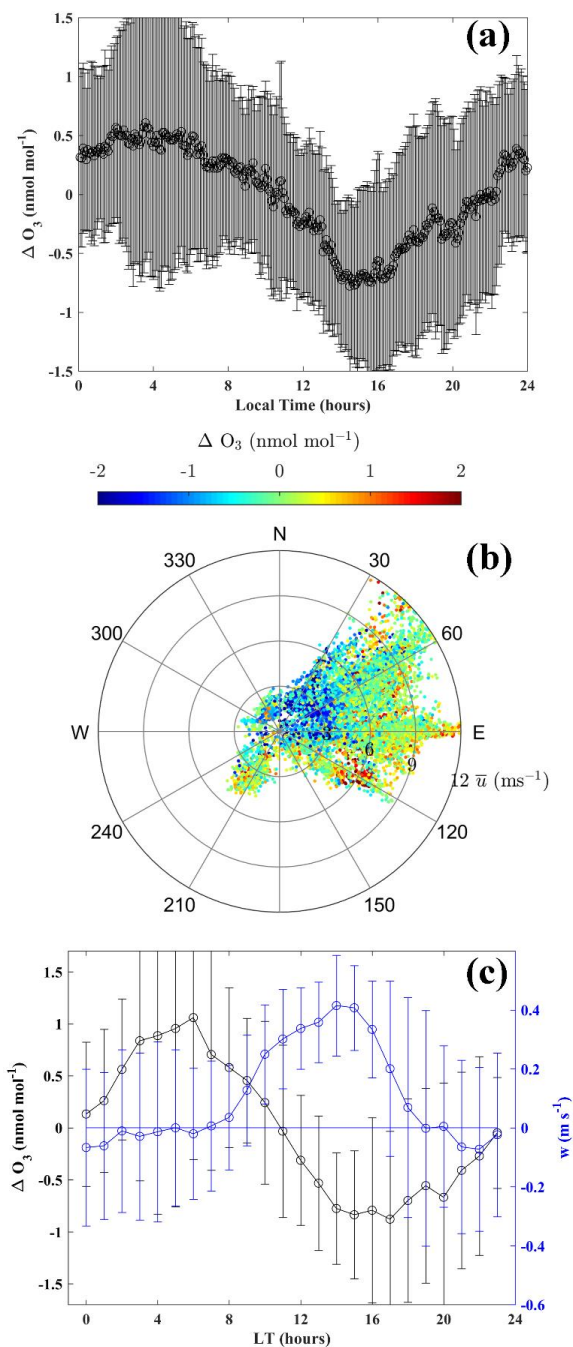


Figure 9. (a) Diurnal variation of ΔO_3 , (b) wind rose color coded with ΔO_3 , and (c) variation in collocated vertical wind and ΔO_3 at Bharati during the austral summer of 2016.



455 Diurnal patterns with an amplitude ranging from ~ 0.2 – 2 nmol mol^{-1} were reported at coastal
(Syowa and McMurdo) and inland Concordia (75° S; 123° E; 3220 m above sea level) stations
(Ghude et al., 2006; Legrand et al., 2009). However, such a pattern is absent over the South Pole
(Oltmans, 1981). Interestingly, photochemical production during the morning hours (05:00–11:00)
due to the NO_x released from snow was followed by a reduction due to an increase in boundary
460 layer height (200 ± 100 m) at the inland station Concordia (Legrand et al., 2009; 2016). Shallow
convective boundary layers (less than 300 m) were reported over the Antarctic Plateau region by
Mastrantonio et al. (1999). Unlike these studies, we did not observe photochemical O_3 production
nor a clear signature of changes in O_3 transport across the top of boundary layer from our
ozonesonde measured O_3 profiles over Bharati station. Therefore, the diurnal patterns of O_3 over
465 coastal Antarctica are found to be different than those over the inland region, mainly due to
differences in meteorological conditions and the concentrations of precursor gases.

3.5 Absence of signature of halogen chemistry

Reactive halogens (e.g., iodine, bromine) have been shown to deplete O_3 in the boundary
layer over the Antarctic region (Barrie et al., 1988; Oltmans and Komhyr, 1976). However,
470 ground-based remote sensing observations found very low concentrations of iodine oxide
($\sim 0.3 \pm 0.1$ pmol mol^{-1}) in the boundary layer over Bharati station during the study period (Mahajan
et al., 2021) and no clear sign of O_3 depletion was observed.

Satellite (SCIAMACHY—SCanning Imaging Absorption spectroMeter for Atmospheric
Cartography and OMI—Ozone Monitoring Instrument) observations also show lower monthly
475 mean iodine monoxide (IO) columnar density (0 – 1×10^{12} molecules cm^{-2}) over Bharati compared
to west Antarctica (figure not shown). This is consistent with previous studies (e.g., Schönhardt et
al., 2012) showing relatively low IO over east Antarctica and the adjacent ocean ($\leq 0.7 \times 10^{12}$
molecules cm^{-2}) compared to west Antarctica ($\sim 1.5 \times 10^{12}$ molecules cm^{-2}) during summer season
(December-January-February 2004–2009).

480 Bromine (Br) driven O_3 depletion events, resulting into BrO, are less frequent over the
Antarctic region compared to the Arctic region due to differences in springtime surface
temperatures (Tarasick and Bottenheim, 2002). However, large O_3 depletion events were observed



at Neumayer (70.62° S, 8.37° W; 42 m amsl) during the late winter (July to September), likely due to stronger BrO episodes from the larger sea ice coverage around the site (Legrand et al., 2009).
485 Analysis of BrO from OMI possibly indicates an O₃ depletion event on 7 February 2015 at Bharati where BrO was enhanced, $\sim 9.2 \times 10^{13}$ molecules cm⁻² with lower O₃ (~ 7 nmol mol⁻¹), marked by red rectangle in Fig. S8. Except for this event, BrO remained below 8×10^{13} molecules cm⁻² around Bharati station ($\pm 0.5^\circ$ latitude/longitude) during the study. O₃ depletion was also not seen at Syowa (Fig. S9) during the study period. The coastal region of east Antarctica exhibits slightly higher
490 values of BrO ($\sim 7 \times 10^{13}$ molecules cm⁻²) compared to the ocean and land regions ($4\text{--}6 \times 10^{13}$ molecules cm⁻²). However, it is low ($4\text{--}8 \times 10^{13}$ molecules cm⁻²) during December–February (2004–2009) compared to the levels during September–November ($5\text{--}10 \times 10^{13}$ molecules cm⁻²) over the Antarctic region (Schönhardt et al., 2012). The impact of Br chemistry on surface O₃ is suggested to be weaker along the east coast of Antarctica (Dumont d’Urville and Syowa) in
495 contrast to western coastal Antarctica as observed over the Neumayer and Halley (75.55° S, 26.53° W, 30 m amsl) stations (Legrand et al., 2016). Nevertheless, simultaneous measurements of O₃ and halogen species including BrO are desirable to quantify the role of halogen chemistry over eastern Antarctica.

3.6 Surface O₃ during winter

500 To take into account the seasonality of O₃ at the surface, the wintertime distribution is shown in Fig. S10. Mean surface O₃ level is higher during winter (20–32 nmol mol⁻¹) compared to the summer (11–23 nmol mol⁻¹), in line with the reported seasonality in the literature (Legrand et al., 2009). Figure S10 reveals three low-O₃ patches over the coastal oceanic region. One is close to Bharati station, however, we do not have observations during wintertime for comparison. Model
505 simulations suggest that surface O₃ is composed of 63–67% O₃s of stratospheric origin during winter (Fig. S10b), which is significantly higher than during austral summer. The probability of downward transport from the stratosphere during winter, also associated with a lower altitude of the tropopause, is larger (Kumar et al., 2021). Comparison of surface O₃ at Syowa (69.00 °S; 39.58 °E; not shown here) shows that the model captures the variability with R=0.3 and a negative bias
510 of ~ 5 nmol mol⁻¹. The model performance seems to be better during summer, indicative of limitations to reproduce the mean O₃ concentrations and the variability during winter. Analysis of the O₃ budget suggests a small net loss of O₃ by 10–25 pmol mol⁻¹ d⁻¹ over the oceanic region and



close to zero ($<5 \text{ pmol mol}^{-1} \text{ d}^{-1}$) over the Antarctic continent (Fig. S11). To study this in greater detail, we highly recommend to conduct continuous wintertime measurements of O_3 , its precursors including halogens over Bharati during winter season.

4 Summary

Ground- and balloon-borne O_3 measurements have been conducted over the Indian station Bharati at the east coast of Antarctica during the austral summers of 2015–2017. The observations have been used to evaluate the performance of the global chemistry-climate model EMAC over this part of the world. A comprehensive analysis of observations and model simulations provided significant insights into the dynamical and photochemical processes affecting surface O_3 and its variability. The main results are:

1. Surface O_3 levels over the Indian station Bharati at the eastern coastal Antarctica have been observed to be $\sim 19 \text{ nmol mol}^{-1}$ with a small variability of $\sim 2 \text{ nmol mol}^{-1}$ during austral summer. While similar levels prevail over the east coast, O_3 is typically higher over land at higher elevation. EMAC model successfully reproduced the observed mean levels with negligible bias over this unique environment and also captured the temporal variability ($R=0.5$). In particular, the model successfully reproduced some events during which O_3 was enhanced. Analysis of the stratospheric O_3 tracer in the model suggests that 40–50% of surface O_3 is of stratospheric origin with larger fractions over the higher elevation regions in Antarctica.
2. The model successfully reproduced the mean vertical distribution of O_3 over Bharati observed by balloon-borne soundings. Detailed analysis combining the balloon profiles, model tracers, and air mass trajectories shows that downward transport caused the observed events during which O_3 was enhanced.
3. Along the east coast of Antarctica, including Bharati station, photochemistry acts as a relatively strong sink of surface O_3 ($\sim 190 \text{ pmol mol}^{-1} \text{ d}^{-1}$) when compared to adjacent land and ocean regions. Chemical loss through O_3 photolysis (followed by $\text{H}_2\text{O}+\text{O}(^1\text{D})$) and O_3+HO_2 dominates over the major production (through $\text{NO}+\text{HO}_2$ and $\text{NO}+\text{CH}_3\text{O}_2$). Reverse latitudinal gradients between H_2O and $\text{O}(^1\text{D})$ lead to maximum O_3 loss at the coastal region. The continuous chemical loss is found to be counterbalanced by downward O_3 transport from above. The findings show the intertwined roles of dynamics and photochemistry that govern the O_3



variability over east Antarctica, and maintaining significant O₃ levels despite the absence of local precursor sources.

4. In addition to the role of photochemistry, the diurnal variation of O₃ at Bharati was found to
545 correlate with the diurnal wind changes. Surface O₃ varied with a diurnal amplitude of 1.2 nmol
mol⁻¹, with the higher levels occurring when the wind blew parallel to the coast or from land
regions. In addition, up- and downdrafts also play a role in the diurnal variation.

Our observations during austral summer over three years complement available data e.g.
550 from eastern coastal Antarctica. The observations, besides revealing diurnal and day-to-day
variability, helped in evaluating the performance of a global chemistry-climate model over this
unique, pristine environment. The study provides valuable insights into the complementary roles
of photochemistry and dynamics in governing O₃ and its variability over Antarctica. In view of
increasing anthropogenic activities and the changing climate, monitoring of O₃ and related species
555 (NO, NO₂, CO, VOCs and halogens) is needed.

Code availability. The Modular Earth Submodel System (MESSy) is continuously further
developed and applied by a consortium of institutions. The usage of MESSy and access to the
560 source code is licensed to all affiliates of institutions that are members of the MESSy Consortium.
Institutions can become a member of the MESSy Consortium by signing the MESSy Memorandum
of Understanding. More information can be found on the MESSy Consortium Website
(<http://www.messy-interface.org>, last access: 04 July 2023). The code presented here has been
based on MESSy version 2.55 and is available as git commit #a5bd54d5b in the MESSy repository.

565

Data availability. Measured ozone and EMAC simulated fields shown in the figures can be
obtained from the website of Space Physics Laboratory ([https://spl.gov.in/SPL/index.php/spl-
metadata/104-spl/550-trace-gases-metadata](https://spl.gov.in/SPL/index.php/spl-metadata/104-spl/550-trace-gases-metadata)) or from the direct link,
[https://spl.gov.in/SPL/images/SPL-METADATA/Ozone_Bharati_Antarctica_Summer_2015-
2017.xlsx](https://spl.gov.in/SPL/images/SPL-METADATA/Ozone_Bharati_Antarctica_Summer_2015-2017.xlsx).
570



Author contributions. I.A. Girach conceptualized and designed the study, performed measurements and analysed the datasets. K.V. Subrahmanyam, Koushik N., Mohammed Nazeer M., N.V.P. Kiran Kumar contributed in the measurements. A. Pozzer performed the model
575 simulations. N. Ojha, A. Pozzer, P.R. Nair, S.S. Babu and J. Lelieveld helped I. A. Girach in the analysis and interpretation of the results. I. A. Girach wrote the manuscript and all the co-authors contributed to the review and editing.

Declaration of competing interest. At least one of the (co-)authors is a member of the editorial
580 board of Atmospheric Chemistry and Physics.

Acknowledgements. We gratefully acknowledge the organiser, Centre for Polar and Ocean Research (NCPOR), Goa, Ministry of Earth Sciences, India for providing the opportunity to participate in the 34th, 35th and 36th Indian Scientific Expedition to Antarctica (ISEA). We also
585 acknowledge the leaders of Bharati Station and Voyage for providing necessary support for the smooth conduct of experiments at Bharati station. We are really thankful to Mr. Santosh Muralidharan, Space Physics Laboratory; Mr. Brijesh Desai, Laboratory in-charge of Bharati station during 35th expedition and other expedition members of 34th, 35th and 36th ISEA for their help during the field measurements. We are also thankful to India Meteorological Department
590 (IMD) for providing meteorological observations, hydrogen gas cylinders for balloon ascents and for the help during balloon launches. The EMAC model simulations have been performed at the German Climate Computing Centre (DKRZ). Surface ozone observations at Antarctic stations (South Pole, United States; Arrival Heights, New Zealand; Marambio, Argentina; Syowa, Japan) were obtained from the newly established World Data Centre for Reactive Gases (WDCRG),
595 WMO's GAW (Global Atmosphere Watch; World Meteorological Organization) programme (<https://ebas.nilu.no/> and <https://ebas-data.nilu.no/Default.aspx>). Vertical O₃ profiles measured at Davis station were obtained from <https://woudc.org/data/explore.php>. We highly acknowledge teams of researchers who made ozone measurements at various Antarctic stations and made them available publically. We also acknowledge the NOAA Air Resources Laboratory (ARL) for
600 providing air mass trajectory from the HYSPLIT transport and dispersion model from their READY website (<http://www.arl.noaa.gov/ready.php>).



References

- 605 Ali, K., Trivedi, D. K., and Sahu, S. K.: Surface ozone characterization at Larsemann Hills and Maitri, Antarctica, *Sci. Total Environ.*, 584–585, 1130–1137, <https://doi.org/10.1016/j.scitotenv.2017.01.173>, 2017.
- Barrie, L. A., Bottenheim, J. W., Schnell, R. C., Crutzen, P. J., and Rasmussen, R. A.: Ozone destruction and photochemical reactions at polar sunrise in the lower Arctic atmosphere, *Nature*, 610 334, 138–141, <https://doi.org/10.1038/334138a0>, 1988.
- Bartusek, S., Wu, Y., Ting, M., Zheng, C., Fiore, A., Sprenger, M., and Flemming, J.: Higher-Resolution Tropopause Folding Accounts for More Stratospheric Ozone Intrusions, *Geophys. Res. Lett.*, 50, e2022GL101690, <https://doi.org/10.1029/2022GL101690>, 2023.
- Bloss, W. J., Camredon, M., Lee, J. D., Heard, D. E., Plane, J. M. C., Saiz-Lopez, A., J.-B. 615 Bauguitte, S., Salmon, R. A., and Jones, A. E.: Coupling of HO_x, NO_x and halogen chemistry in the antarctic boundary layer, *Atmos. Chem. Phys.*, 10, 10187–10209, <https://doi.org/10.5194/acp-10-10187-2010>, 2010.
- Brühl, C., Schallack, J., Klingmüller, K., Robert, C., Bingen, C., Clarisse, L., Heckel, A., North, P., and Rieger, L.: Stratospheric aerosol radiative forcing simulated by the chemistry climate 620 model EMAC using Aerosol CCI satellite data, *Atmos. Chem. Phys.*, 18, 12845–12857, <https://doi.org/10.5194/acp-18-12845-2018>, 2018.
- Crawford, J. H., Davis, D. D., Chen, G., Buhr, M., Oltmans, S., Weller, R., Mauldin, L., Eisele, F., Shetter, R., Lefer, B., Arimoto, R., and Hogan, A.: Evidence for photochemical production of ozone at the South Pole surface, *Geophys. Res. Lett.*, 28, 3641–3644, 625 <https://doi.org/10.1029/2001GL013055>, 2001.
- Cristofanelli, P., Putero, D., Bonasoni, P., Busetto, M., Calzolari, F., Camporeale, G., Grigioni, P., Lupi, A., Petkov, B., Traversi, R., Udusti, R., and Vitale, V.: Analysis of multi-year near-surface ozone observations at the WMO/GAW “Concordia” station (75°06’S, 123°20’E, 3280 m a.s.l. –



- Antarctica), *Atmos. Environ.*, 177, 54–63, <https://doi.org/10.1016/j.atmosenv.2018.01.007>, 2018.
- 630 Das, S. S., Ramkumar, G., Koushik, N., Murphy, D. J., Girach, I. A., Suneeth, K. V., Subrahmanyam, K. V., Soni, V. K., Kumar, V., and Nazeer, M.: Multiplatform observations of stratosphere-troposphere exchange over the Bharati (69.41° S, 76° E), Antarctica during ISEA-35, *J. Atmos. Solar-Terrestrial Phys.*, 211, <https://doi.org/10.1016/j.jastp.2020.105455>, 2020.
- Davis, D. D., Eisele, F., Chen, G., Crawford, J., Huey, G., Tanner, D., Slusher, D., Mauldin, L.,
635 Oncley, S., Lenschow, D., Semmer, S., Shetter, R., Lefer, B., Arimoto, R., Hogan, A., Grube, P., Lazzara, M., Bandy, A., Thornton, D., Berresheim, H., Bingemer, H., Hutterli, M., McConnell, J., Bales, R., Dibb, J., Buhr, M., Park, J., McMurry, P., Swanson, A., Meinardi, S., and Blake, D.: An overview of ISCAT 2000, *Atmos. Environ.*, 38, 5363–5373, <https://doi.org/10.1016/j.atmosenv.2004.05.037>, 2004.
- 640 Ding, M., Tian, B., Ashley, M. C. B., Putero, D., Zhu, Z., Wang, L., Yang, S., Li, C., and Xiao, C.: Year-round record of near-surface ozone and O₃ enhancement events (OEEs) at Dome A, East Antarctica, *Earth Syst. Sci. Data*, 12, 3529–3544, <https://doi.org/10.5194/essd-12-3529-2020>, 2020.
- Eisele, F., Davis, D., Helmig, D., Oltmans, S., Neff, W., Huey, G., Tanner, D., Chen, G., Crawford,
645 J., and Arimoto, R.: Antarctic Tropospheric Chemistry Investigation (ANTCI) 2003 overview, *Atmos. Environ.*, 42, 2749–2761, <https://doi.org/10.1016/j.atmosenv.2007.04.013>, 2008.
- Fernandez, R. P., Carmona-Balea, A., Cuevas, C. A., Barrera, J. A., Kinnison, D. E., Lamarque, J.-F., Blaszcak-Boxe, C., Kim, K., Choi, W., Hay, T., Blechschmidt, A.-M., Schönhardt, A., Burrows, J. P., and Saiz-Lopez, A.: Modeling the Sources and Chemistry of Polar Tropospheric
650 Halogens (Cl, Br, and I) Using the CAM-Chem Global Chemistry-Climate Model, *J. Adv. Model. Earth Syst.*, 11, 2259–2289, <https://doi.org/10.1029/2019MS001655>, 2019.
- Frey, M. M., Stewart, R. W., McConnell, J. R., and Bales, R. C.: Atmospheric hydroperoxides in West Antarctica: Links to stratospheric ozone and atmospheric oxidation capacity, *J. Geophys. Res.*, 110, D23301, <https://doi.org/10.1029/2005JD006110>, 2005.
- 655 Frey, M. M., Roscoe, H. K., Kukui, A., Savarino, J., France, J. L., King, M. D., Legrand, M., and Preunkert, S.: Atmospheric nitrogen oxides (NO and NO₂) at Dome C, East Antarctica, during the



OPALE campaign, *Atmos. Chem. Phys.*, 15, 7859–7875, <https://doi.org/10.5194/acp-15-7859-2015>, 2015.

660 Ghude, S. D., Jain, S. L., Arya, B. C., Kulkarni, P. S., Kumar, A., and Ahmed, N.: Temporal and spatial variability of surface ozone at Delhi and Antarctica, *Int. J. Climatol.*, 26, 2227–2242, <https://doi.org/10.1002/joc.1367>, 2006.

Greenslade, J. W., Alexander, S. P., Schofield, R., Fisher, J. A., and Klekociuk, A. K.: Stratospheric ozone intrusion events and their impacts on tropospheric ozone in the Southern Hemisphere, *Atmos. Chem. Phys.*, 17, 10269–10290, <https://doi.org/10.5194/acp-17-10269-2017>, 665 2017.

Griffiths, P. T., Murray, L. T., Zeng, G., Shin, Y. M., Abraham, N. L., Archibald, A. T., Deushi, M., Emmons, L. K., Galbally, I. E., Hassler, B., Horowitz, L. W., Keeble, J., Liu, J., Moeini, O., Naik, V., O’Connor, F. M., Oshima, N., Tarasick, D., Tilmes, S., Turnock, S. T., Wild, O., Young, P. J., and Zanis, P.: Tropospheric ozone in CMIP6 simulations, *Atmos. Chem. Phys.*, 21, 4187–670 4218, <https://doi.org/10.5194/acp-21-4187-2021>, 2021.

Helmig, D., Ganzeveld, L., Butler, T., and Oltmans, S. J.: The role of ozone atmosphere-snow gas exchange on polar, boundary-layer tropospheric ozone – a review and sensitivity analysis, *Atmos. Chem. Phys.*, 7, 15–30, <https://doi.org/10.5194/acp-7-15-2007>, 2007.

Jefferson, A., Tanner, D. J., Eisele, F. L., Davis, D. D., Chen, G., Crawford, J., Huey, J. W., Torres, 675 A. L., and Berresheim, H.: OH photochemistry and methane sulfonic acid formation in the coastal Antarctic boundary layer, *J. Geophys. Res. Atmos.*, 103, 1647–1656, <https://doi.org/10.1029/97JD02376>, 1998.

Jöckel, P., Tost, H., Pozzer, A., Brühl, C., Buchholz, J., Ganzeveld, L., Hoor, P., Kerkweg, A., Lawrence, M. G., Sander, R., Steil, B., Stiller, G., Tanarhte, M., Taraborrelli, D., van Aardenne, 680 J., and Lelieveld, J.: The atmospheric chemistry general circulation model ECHAM5/MESSy1: consistent simulation of ozone from the surface to the mesosphere, *Atmos. Chem. Phys.*, 6, 5067–5104, <https://doi.org/10.5194/acp-6-5067-2006>, 2006.

Jöckel, P., Kerkweg, A., Pozzer, A., Sander, R., Tost, H., Riede, H., Baumgaertner, A., Gromov, S., and Kern, B.: Development cycle 2 of the Modular Earth Submodel System (MESSy2), *Geosci.*



685 Model Dev., 3, 717–752, <https://doi.org/10.5194/gmd-3-717-2010>, 2010.

Jöckel, P., Tost, H., Pozzer, A., Kunze, M., Kirner, O., Brenninkmeijer, C. A. M., Brinkop, S., Cai, D. S., Dyroff, C., Eckstein, J., Frank, F., Garny, H., Gottschaldt, K.-D., Graf, P., Grewe, V., Kerkweg, A., Kern, B., Matthes, S., Mertens, M., Meul, S., Neumaier, M., Nützel, M., Oberländer-Hayn, S., Ruhnke, R., Runde, T., Sander, R., Scharffe, D., and Zahn, A.: Earth System Chemistry
690 integrated Modelling (ESCiMo) with the Modular Earth Submodel System (MESSy) version 2.51, Geosci. Model Dev., 9, 1153–1200, <https://doi.org/10.5194/gmd-9-1153-2016>, 2016.

Jones, A. E.: An analysis of the oxidation potential of the South Pole boundary layer and the influence of stratospheric ozone depletion, J. Geophys. Res., 108, 4565, <https://doi.org/10.1029/2003JD003379>, 2003.

695 Jones, A. E., Weller, R., Anderson, P. S., Jacobi, H.-W., Wolff, E. W., Schrems, O., and Miller, H.: Measurements of NO_x emissions from the Antarctic snowpack, Geophys. Res. Lett., 28, 1499–1502, <https://doi.org/10.1029/2000GL011956>, 2001.

Jones, A. E., Wolff, E. W., Salmon, R. A., Bauguitte, S. J.-B., Roscoe, H. K., Anderson, P. S., Ames, D., Clemitshaw, K. C., Fleming, Z. L., Bloss, W. J., Heard, D. E., Lee, J. D., Read, K. A.,
700 Hamer, P., Shallcross, D. E., Jackson, A. V., Walker, S. L., Lewis, A. C., Mills, G. P., Plane, J. M. C., Saiz-Lopez, A., Sturges, W. T., and Worton, D. R.: Chemistry of the Antarctic Boundary Layer and the Interface with Snow: an overview of the CHABLIS campaign, Atmos. Chem. Phys., 8, 3789–3803, <https://doi.org/10.5194/acp-8-3789-2008>, 2008.

Jones, A. E., Wolff, E. W., Brough, N., Bauguitte, S. J.-B., Weller, R., Yela, M., Navarro-Comas,
705 M., Ochoa, H. A., and Theys, N.: The spatial scale of ozone depletion events derived from an autonomous surface ozone network in coastal Antarctica, Atmos. Chem. Phys., 13, 1457–1467, <https://doi.org/10.5194/acp-13-1457-2013>, 2013.

Kukui, A., Legrand, M., Ancellet, G., Gros, V., Bekki, S., Sarda-Estève, R., Loisil, R., and Preunkert, S.: Measurements of OH and RO₂ radicals at the coastal Antarctic site of Dumont
710 d’Urville (East Antarctica) in summer 2010–2011, J. Geophys. Res. Atmos., 117, <https://doi.org/10.1029/2012JD017614>, 2012.

Kumar, P., Kuttippurath, J., von der Gathen, P., Petropavlovskikh, I., Johnson, B., McClure-



- 715 Begley, A., Cristofanelli, P., Bonasoni, P., Barlasina, M. E., and Sánchez, R.: The Increasing Surface Ozone and Tropospheric Ozone in Antarctica and Their Possible Drivers, *Environ. Sci. Technol.*, *55*, 8542–8553, <https://doi.org/10.1021/acs.est.0c08491>, 2021.
- Legrand, M., Preunkert, S., Jourdain, B., Gallée, H., Goutail, F., Weller, R., and Savarino, J.: Year-round record of surface ozone at coastal (Dumont d’Urville) and inland (Concordia) sites in East Antarctica, *J. Geophys. Res. Atmos.*, *114*, <https://doi.org/10.1029/2008JD011667>, 2009.
- 720 Legrand, M., Preunkert, S., Savarino, J., Frey, M. M., Kukui, A., Helmig, D., Jourdain, B., Jones, A. E., Weller, R., Brough, N., and Gallée, H.: Inter-annual variability of surface ozone at coastal (Dumont d’Urville, 2004–2014) and inland (Concordia, 2007–2014) sites in East Antarctica, *Atmos. Chem. Phys.*, *16*, 8053–8069, <https://doi.org/10.5194/acp-16-8053-2016>, 2016.
- Lelieveld, J. and Dentener, F. J.: What controls tropospheric ozone?, *J. Geophys. Res. Atmos.*, *105*, 3531–3551, <https://doi.org/10.1029/1999JD901011>, 2000.
- 725 Lelieveld, J., van Aardenne, J., Fischer, H., de Reus, M., Williams, J., and Winkler, P.: Increasing Ozone over the Atlantic Ocean, *Science*, *304*, 1483–1487, <https://doi.org/10.1126/science.1096777>, 2004.
- Mahajan, A. S., Li, Q., Inamdar, S., Ram, K., Badia, A., and Saiz-Lopez, A.: Modelling the impacts of iodine chemistry on the northern Indian Ocean marine boundary layer, *Atmos. Chem. Phys.*, *21*, 8437–8454, <https://doi.org/10.5194/acp-21-8437-2021>, 2021.
- 730 Masclin, S., Frey, M. M., Rogge, W. F., and Bales, R. C.: Atmospheric nitric oxide and ozone at the WAIS Divide deep coring site: a discussion of local sources and transport in West Antarctica, *Atmos. Chem. Phys.*, *13*, 8857–8877, <https://doi.org/10.5194/acp-13-8857-2013>, 2013.
- Mastrantonio, G., Malvestuto, V., Argentini, S., Georgiadis, T., and Viola, A.: Evidence of a Convective Boundary Layer Developing on the Antarctic Plateau during the Summer, *Meteorol. Atmos. Phys.*, *71*, 127–132, <https://doi.org/10.1007/s007030050050>, 1999.
- Mihalikova, M. and Kirkwood, S.: Tropopause fold occurrence rates over the Antarctic station Troll (72° S, 2.5° E), *Ann. Geophys.*, *31*, 591–598, <https://doi.org/10.5194/angeo-31-591-2013>, 2013.



740 Morgenstern, O., Zeng, G., Luke Abraham, N., Telford, P. J., Braesicke, P., Pyle, J. A., Hardiman, S. C., O'Connor, F. M., and Johnson, C. E.: Impacts of climate change, ozone recovery, and increasing methane on surface ozone and the tropospheric oxidizing capacity, *J. Geophys. Res. Atmos.*, 118, 1028–1041, <https://doi.org/10.1029/2012JD018382>, 2013.

Murayama, S., Nakazawa, T., Tanaka, M., Aoki, S., and Kawaguchi, S.: Variations of tropospheric ozone concentration over Syowa Station, Antarctica, *Tellus B Chem. Phys. Meteorol.*, <https://doi.org/10.3402/tellusb.v44i4.15454>, 1992.

Murazaki, K. and Hess, P.: How does climate change contribute to surface ozone change over the United States?, *J. Geophys. Res. Atmos.*, 111, <https://doi.org/10.1029/2005JD005873>, 2006.

750 Nguyen, D.-H., Lin, C., Vu, C.-T., Cheruiyot, N. K., Nguyen, M. K., Le, T. H., Lukkhasorn, W., Vo, T.-D.-H., and Bui, X.-T.: Tropospheric ozone and NO_x: A review of worldwide variation and meteorological influences, *Environ. Technol. Innov.*, 28, 102809, <https://doi.org/10.1016/j.eti.2022.102809>, 2022.

Ojha, N., Pozzer, A., Akritidis, D., and Lelieveld, J.: Secondary ozone peaks in the troposphere over the Himalayas, *Atmos. Chem. Phys.*, 17, 6743–6757, <https://doi.org/10.5194/acp-17-6743-2017>, 2017.

Oltmans, S. J.: Surface ozone measurements in clean air, *J. Geophys. Res. Ocean.*, 86, 1174–1180, <https://doi.org/10.1029/JC086iC02p01174>, 1981.

Oltmans, S. J. and Komhyr, W. D.: Surface ozone in Antarctica, *J. Geophys. Res.*, 81, 5359–5364, <https://doi.org/10.1029/JC081i030p05359>, 1976.

760 Oltmans, S. J., Johnson, B. J., and Helmig, D.: Episodes of high surface-ozone amounts at South Pole during summer and their impact on the long-term surface-ozone variation, *Atmos. Environ.*, 42, 2804–2816, <https://doi.org/10.1016/j.atmosenv.2007.01.020>, 2008.

765 Pozzer, A., de Meij, A., Pringle, K. J., Tost, H., Doering, U. M., van Aardenne, J., and Lelieveld, J.: Distributions and regional budgets of aerosols and their precursors simulated with the EMAC chemistry-climate model, *Atmos. Chem. Phys.*, 12, 961–987, <https://doi.org/10.5194/acp-12-961-2012>, 2012.



Pozzer, A., Reifenberg, S. F., Kumar, V., Franco, B., Kohl, M., Taraborrelli, D., Gromov, S., Ehrhart, S., Jöckel, P., Sander, R., Fall, V., Rosanka, S., Karydis, V., Akritidis, D., Emmerichs, T., Crippa, M., Guizzardi, D., Kaiser, J. W., Clarisse, L., Kiendler-Scharr, A., Tost, H., and Tsimpidi, A.: Simulation of organics in the atmosphere: evaluation of EMACv2.54 with the Mainz Organic Mechanism (MOM) coupled to the ORACLE (v1.0) submodel, *Geosci. Model Dev.*, 15, 2673–2710, <https://doi.org/10.5194/gmd-15-2673-2022>, 2022.

Preunkert, S., Ancellet, G., Legrand, M., Kukui, A., Kerbrat, M., Sarda-Estève, R., Gros, V., and Jourdain, B.: Oxidant Production over Antarctic Land and its Export (OPALE) project: An overview of the 2010–2011 summer campaign, *J. Geophys. Res. Atmos.*, 117, <https://doi.org/10.1029/2011JD017145>, 2012.

Reddy, N. S. K., N.V.P., K., K., R. G., G., B., and K., R. R.: Characteristics of atmospheric surface layer during winter season over Anantapur (14.62° N, 77.65° E), a semi-arid location in peninsular India, *J. Atmos. Solar-Terrestrial Phys.*, 216, 105554, <https://doi.org/10.1016/j.jastp.2021.105554>, 2021.

Reifenberg, S. F., Martin, A., Kohl, M., Bacer, S., Hamryszczak, Z., Tadic, I., Röder, L., Crowley, D. J., Fischer, H., Kaiser, K., Schneider, J., Dörich, R., Crowley, J. N., Tomsche, L., Marsing, A., Voigt, C., Zahn, A., Pöhlker, C., Holanda, B. A., Krüger, O., Pöschl, U., Pöhlker, M., Jöckel, P., Dorf, M., Schumann, U., Williams, J., Bohn, B., Curtius, J., Harder, H., Schlager, H., Lelieveld, J., and Pozzer, A.: Numerical simulation of the impact of COVID-19 lockdown on tropospheric composition and aerosol radiative forcing in Europe, *Atmos. Chem. Phys.*, 22, 10901–10917, <https://doi.org/10.5194/acp-22-10901-2022>, 2022.

Roeckner, E., Brokopf, R., Esch, M., Giorgetta, M., Hagemann, S., Kornblueh, L., Manzini, E., Schlese, U., and Schulzweida, U.: Sensitivity of Simulated Climate to Horizontal and Vertical Resolution in the ECHAM5 Atmosphere Model, *J. Clim.*, 19, 3771–3791, <https://doi.org/10.1175/JCLI3824.1>, 2006.

Rolph, G., Stein, A., and Stunder, B.: Real-time Environmental Applications and Display sYstem: READY, *Environ. Model. Softw.*, 95, 210–228, <https://doi.org/10.1016/j.envsoft.2017.06.025>, 2017.



795 Saiz-Lopez, A., Mahajan, A. S., Salmon, R. A., Bauguitte, S. J.-B., Jones, A. E., Roscoe, H. K.,
and Plane, J. M. C.: Boundary Layer Halogens in Coastal Antarctica, *Science*, 317, 348–351,
<https://doi.org/10.1126/science.1141408>, 2007.

Sanak, J., Lambert, G., and Ardouin, B.: Measurement of stratosphere-to-troposphere exchange in
Antarctica by using short-lived cosmonuclides, *Tellus B Chem. Phys. Meteorol.*,
800 <https://doi.org/10.3402/tellusb.v37i2.15005>, 1985.

Schönhardt, A., Begoin, M., Richter, A., Wittrock, F., Kaleschke, L., Gómez Martín, J. C., and
Burrows, J. P.: Simultaneous satellite observations of IO and BrO over Antarctica, *Atmos. Chem.
Phys.*, 12, 6565–6580, <https://doi.org/10.5194/acp-12-6565-2012>, 2012.

Seinfeld, J. H. and Pandis, S. N.: Atmospheric Chemistry and Physics: From Air Pollution to
805 Climate Change, 88–90 pp., <https://doi.org/10.1063/1.882420>, 1998.

Simpson, W. R., von Glasow, R., Riedel, K., Anderson, P., Ariya, P., Bottenheim, J., Burrows, J.,
Carpenter, L. J., Frieß, U., Goodsite, M. E., Heard, D., Hutterli, M., Jacobi, H.-W., Kaleschke, L.,
Neff, B., Plane, J., Platt, U., Richter, A., Roscoe, H., Sander, R., Shepson, P., Sodeau, J., Steffen,
A., Wagner, T., and Wolff, E.: Halogens and their role in polar boundary-layer ozone depletion,
810 *Atmos. Chem. Phys.*, 7, 4375–4418, <https://doi.org/10.5194/acp-7-4375-2007>, 2007.

Soni, V. K., Sateesh, M., Das, A. K., and Peshin, S. K.: Progress in meteorological studies around
Indian stations in Antarctica, *Proc. Indian Natl. Sci. Acad.*, 83,
<https://doi.org/10.16943/ptinsa/2017/48954>, 2017.

Stein, A. F., Draxler, R. R., Rolph, G. D., Stunder, B. J. B., Cohen, M. D., and Ngan, F.: NOAA's
815 HYSPLIT Atmospheric Transport and Dispersion Modeling System, *Bull. Am. Meteorol. Soc.*,
96, 2059–2077, <https://doi.org/10.1175/BAMS-D-14-00110.1>, 2015.

Stohl, A., Bonasoni, P., Cristofanelli, P., Collins, W., Feichter, J., Frank, A., Forster, C.,
Gerasopoulos, E., Gäggeler, H., James, P., Kentarchos, T., Kromp-Kolb, H., Krüger, B., Land, C.,
Meloan, J., Papayannis, A., Priller, A., Seibert, P., Sprenger, M., Roelofs, G. J., Scheel, H. E.,
820 Schnabel, C., Siegmund, P., Tobler, L., Trickl, T., Wernli, H., Wirth, V., Zanis, P., and Zerefos,
C.: Stratosphere-troposphere exchange: A review, and what we have learned from STACCATO,
J. Geophys. Res. Atmos., 108, <https://doi.org/10.1029/2002JD002490>, 2003.



Taraborrelli, D., Cabrera-Perez, D., Bacer, S., Gromov, S., Lelieveld, J., Sander, R., and Pozzer, A.: Influence of aromatics on tropospheric gas-phase composition, *Atmos. Chem. Phys.*, 21, 2615–825 2636, <https://doi.org/10.5194/acp-21-2615-2021>, 2021.

Tarasick, D. W. and Bottenheim, J. W.: Surface ozone depletion episodes in the Arctic and Antarctic from historical ozonesonde records, *Atmos. Chem. Phys.*, 2, 197–205, <https://doi.org/10.5194/acp-2-197-2002>, 2002.

Tian, B., Ding, M., Putero, D., Li, C., Zhang, D., Tang, J., Zheng, X., Bian, L., and Xiao, C.: Multi-830 year variation of near-surface ozone at Zhongshan Station, Antarctica, *Environ. Res. Lett.*, 17, 044003, <https://doi.org/10.1088/1748-9326/ac583c>, 2022.

Wang, H., Lu, X., Jacob, D. J., Cooper, O. R., Chang, K.-L., Li, K., Gao, M., Liu, Y., Sheng, B., Wu, K., Wu, T., Zhang, J., Sauvage, B., Nédélec, P., Blot, R., and Fan, S.: Global tropospheric ozone trends, attributions, and radiative impacts in 1995–2017: an integrated analysis using aircraft 835 (IAGOS) observations, ozonesonde, and multi-decadal chemical model simulations, *Atmos. Chem. Phys.*, 22, 13753–13782, <https://doi.org/10.5194/acp-22-13753-2022>, 2022.

Winkler, P., Brylka, S., and Wagenbach, D.: Regular fluctuations of surface ozone at Georg-von-Neumayer station, Antarctica, *Tellus B*, 44, 33–40, <https://doi.org/10.1034/j.1600-0889.1992.00003.x>, 1992.

840 Yang, X., Cox, R. A., Warwick, N. J., Pyle, J. A., Carver, G. D., O'Connor, F. M., and Savage, N. H.: Tropospheric bromine chemistry and its impacts on ozone: A model study, *J. Geophys. Res. Atmos.*, 110, <https://doi.org/10.1029/2005JD006244>, 2005.

Young, P. J., Naik, V., Fiore, A. M., Gaudel, A., Guo, J., Lin, M. Y., Neu, J. L., Parrish, D. D., Rieder, H. E., Schnell, J. L., Tilmes, S., Wild, O., Zhang, L., Ziemke, J., Brandt, J., Delcloo, A., 845 Doherty, R. M., Geels, C., Hegglin, M. I., Hu, L., Im, U., Kumar, R., Luhar, A., Murray, L., Plummer, D., Rodriguez, J., Saiz-Lopez, A., Schultz, M. G., Woodhouse, M. T., and Zeng, G.: Tropospheric Ozone Assessment Report: Assessment of global-scale model performance for global and regional ozone distributions, variability, and trends, *Elem. Sci. Anthr.*, 6, 10, <https://doi.org/10.1525/elementa.265>, 2018.

850